Multiple-Wavelength Integration in InGaAs–InGaAsP Structures Using Pulsed Laser Irradiation-Induced Quantum-Well Intermixing

Boon Siew Ooi, *Senior Member, IEEE*, Teik Kooi Ong, and Oki Gunawan

***Abstract*—In this paper, we present the characteristics of a quantum-well intermixing technique using pulsed-photoabsorption-induced disordering. Photoluminescence, micro-Raman spectroscopy, and transmission electron microscopy were used to characterize the process. Using this technique, a differential wavelength shift between the intermixed and nonintermixed regions of over 160 nm has been observed from InGaAs–InGaAsP heterostructures. It was found from the micro-Raman measurements that a spatial resolution of better than 2.5 μm can be achieved. A theoretical model has been developed to estimate the spatial resolution limit. Theoretical analysis has also been performed to investigate the effect of laser irradiation on the degree of intermixing in InGaAs–InGaAsP structures. To verify the capability of this process in monolithic photonic integration, high-quality bandgap tuned lasers, two-section extended cavity lasers, and multiple-wavelength laser chips have been fabricated.**

***Index Terms*—InGaAs–InGaAsP, monolithic integration, photonic integrated circuits, pulsed laser irradiation, quantum-well intermixing, quantum-well laser.**

I. Introduction

QUANTUM-WELL intermixing (QWI) has been viewed as one of the promising technologies for the fabrication of photonic integrated circuits (PICs) [1]. To make the QWI process feasible for multiple channels and high-density photonic integration, a process that is capable of producing a multiple-wavelength chip with high spatial selectivity and high material quality is highly desirable. Among the various QWI techniques, a one-step multiple-wavelength process has been developed using impurity-free vacancy diffusion (IFVD) [2], [3] and gray mask ion-implantation induced disordering (IID) [4] techniques. However, these methods involve complex masking and processing steps. For example, the multiple-wavelength process using the gray mask IID method [4] requires a precise control of the SiO_2 implant mask thickness using a one-step lithography and dry etch process. As the degree of intermixing is dependent on the implant dosage; which is controlled by the thickness of the SiO_2 mask, the number of bandgaps that can be obtained using this technique is limited by the SiO_2 thickness and the energy of the ion implantation process.

In this paper, we report a laser direct writing method using pulsed photoabsorption-induced disordering (PPAID) [5] to achieve high-spatial-selectivity multiple-wavelength chip in InGaAs–InGaAsP heterostructures. This process has been successfully developed in InGaAs–InGaAsP material systems [6], [7], as well as in GaAs–AlGaAs quantum-well (QW) structures [8]. It has been shown that a relatively good spatial resolution can be obtained from this technique [9]. In addition, the PPAID process has also been attempted to use to directly create gratings in InGaAs–InGaAsP QW structures [10]. In order to have a better understanding of the process mechanisms, the resolution limit, and the properties of the intermixed structures, we further characterize this QWI process using photoluminescence (PL), micro-Raman spectroscopy, and transmission electron microscopy (TEM). A theoretical model has been developed to estimate the limit of spatial resolution of the PPAID process. Theoretical analysis has also been performed to investigate the relationship between the irradiation conditions and the bandgap shift. Devices such as bandgap tuned lasers, integrated extended cavity lasers, and multiple-wavelength laser chips have also been fabricated and characterized to verify the integration capability of this postgrowth bandgap engineering technique.

II. Photoluminescence Characterization

PPAID involves using a Q-switched Nd:YAG laser with a pulse length of a few nanoseconds and repetition rate of 10 Hz to directly irradiate the sample. The absorption of high-energy pulses from the Nd:YAG laser produces transient heating in the crystal. Rapid thermal expansion will then cause bond breaking and lattice disruption that lead to a localized increase in the density of point defects. Subsequent high-temperature annealing results in diffusion of the point defects and enhances the QWI rate. The laser pulses used were comparable to the thermal time constant of that of InP in order to minimize the effects of lateral diffusion and generate highly localized temperature spikes. In this study, a Q-switched Nd:YAG laser with a wavelength of 1.064 μm, generating pulses of $\sim$8 ns and a pulse repetition rate of 10 Hz was used.

The material used in this study is a laser structure with an emission wavelength of around 1.55 μm. It was grown by metal–organic chemical vapor deposition (MOCVD) on an

Manuscript received September 9, 2003; revised February 3, 2004.

B. S. Ooi is with the Center for Optical Technologies, Department of Electrical and Computer Engineering, Lehigh University, Sinclair Laboratory, Bethlehem, PA 18015 USA (e-mail: bsooi@ieee.org).

T. K. Ong was with the School of Electrical and Electronics Engineering, Nanyang Technological University, Singapore S639798. He is now with Denselight Semiconductor Pte. Ltd., Singapore S498831.

O. Gunawan was with the School of Electrical and Electronics Engineering, Nanyang Technological University, Singapore S639798. He is now with the Department of Electrical Engineering, Princeton University, Princeton, NJ 08544 USA.

Digital Object Identifier 10.1109/JQE.2004.826431

Si-doped (100) InP substrate. The single QW (SQW) region consists of a 55-Å-wide $In_xGa_{1-x}As$ $(x = 0.53)$ active region with 120-Å InGaAsP ($\lambda_g = 1.26\,\mu$m, where λ_g is the room-temperature PL wavelength) barriers. The QW is bounded by a graded index (GRIN) waveguide core consisting of InGaAsP confining layers. The thicknesses and compositions of these layers (from the QWs outward) are 500 Å of $\lambda_g = 1.18\,\mu$m and 800 Å of $\lambda_g = 1.05\,\mu$m. The structure is lattice matched to InP throughout. It is completed with a 1.37-μm InP upper cladding layer and a layer of 0.05-μm InGaAsP ($\lambda_g = 1.18\,\mu$m) followed by 0.1 μm of $In_xGa_{1-x}As$ $(x = 0.53)$. The upper cladding layer (InP) is doped with Zn to a concentration of 7.3×10^{17} cm^{-3}, and the subsequent layers are doped with 2×10^{18} cm^{-3} and 1.8×10^{19} cm^{-3} of Zn, respectively. The thickness of the lower cladding layer (InP) is 1.0 μm and is doped with Si to a concentration of 2.5×10^{18} cm^{-3}. The waveguide core is undoped, hence forming the p-i-n structure with the intrinsic region restricted to the QWs and GRIN layers.

For process characterization, samples 2×2 mm^2 in area were irradiated at room temperature with normal incidence to the surface. The samples were irradiated with pulse energy densities of 2.8, 3.5, and 3.9 mJ·mm^{-2}, respectively, at different exposure times. It is noted that the surface morphology for a sample irradiated with pulsed energy density of >4.0 mJ·mm^{-2} for >5 s will degrade significantly due to laser ablation. The surface of the sample was protected by 200-nm Si_xN_y, deposited using plasma-enhanced chemical vapor deposition (PECVD) during the laser irradiation. This dielectric layer acts as an antireflection coating and a protective layer against the surface reaction with the atmosphere. It also prevents group V desorption during the high-temperature annealing.

After the laser exposure, the samples were annealed at 625 °C in a flowing N_2 ambient for 120 s using a rapid thermal processor (RTP). The RTP condition was obtained from a thermal stability test performed on the as-grown samples. During annealing, the samples were sandwiched between two pieces of fresh GaAs substrates. These proximity caps provide As over pressure, so that diffusion of group V elements from the surface would be minimized during high-temperature annealing. An as-grown sample, which was not exposed to the laser irradiation, was included during the annealing to act as a control sample. PL measurements at 77 K were performed using a 1.064-μm CW Nd:YAG laser beam to study the peak wavelength of the samples before and after laser irradiation as well as after intermixing.

Before annealing, no PL signal could be detected from the front surface of the irradiated samples. However, PL spectra could still be retrieved from the back surface, i.e., from the substrate. The PL peak obtained was identical to that of the as-grown samples. These observations suggest that most of the lattice disruption and bond breaking caused by the laser irradiation were limited to the GRIN layers. These high levels of residual defects act as nonradiative recombination centers, which prohibit the detection of the PL signal.

The bandgap energies of lattice-matched $In_{0.53}Ga_{0.47}$ As and $In_xGa_{1-x}As_yP_{1-y}$ with $\lambda_g = 1.26$ μm and 1.18 μm are 0.72, 0.984, and 1.051 eV, respectively [11]. These bandgaps are smaller than that of the 1.064-μm laser (1.165 eV). Thus, most of the photons will be absorbed by the InGaAs contact and the GRIN layers, leaving behind a low-intensity 1.064-μm beam for the active layer to absorb. The QWI effect of this process is therefore enhanced by the in-diffusion of the point defects in these layers to the QW layer during the annealing stage.

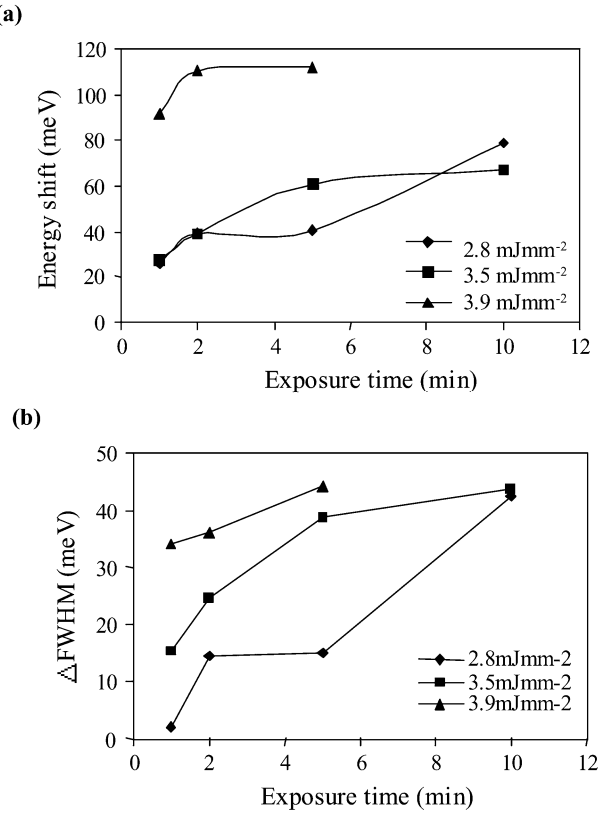

Fig. 1. (a) Energy shift relative to the control sample for samples exposed to different energy densities and exposure times. (b) FWHM relative to the as-grown sample for samples exposed to different energy densities and exposure times.

Fig. 1(a) gives the bandgap energy shift from samples exposed to various laser intensities as a function of exposure time after annealing at 625 °C for 120 s. It can be observed that the bandgap energies of samples subjected to higher pulse energy densities and longer irradiation times have been shifted to a higher bandgap energy. The degree of intermixing was found to saturate for samples irradiated with pulse energy densities higher than 3.5 mJ·mm^{-2} and exposure time longer than 5 min. This might be attributed to the agglomeration of point defects into extended defects such as vacancy clusters, which inhibit diffusion of point defects particularly from the InGaAs contact layer to the QW.

The level of the saturation points varied for samples exposed to different pulse energies. The point defects generated are believed to be proportional to the pulse energy of the laser beam. A higher density of point defects will, therefore, lead to a higher degree of QWI and different levels of saturation. No PL signal can be retrieved for the sample exposed to 3.9 mJ·mm^{-2} for 10 min. This might be attributed to the fact that both the highly absorbing InGaAs contact and the QW regions have been severely damaged by extended defects formed during the laser irradiation.

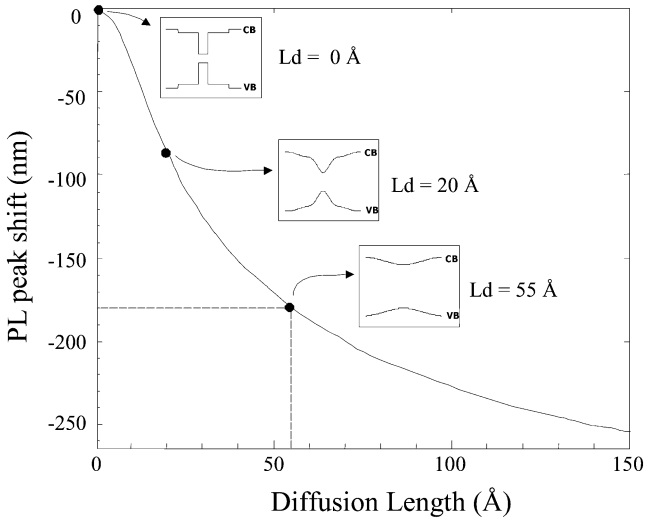

Fig. 2. Calculated PL wavelength shift with respect to the as-grown sample at various diffusion lengths. The insets show the QW bandgap profile for three different group III diffusion lengths.

The full-width at half maximum (FWHM) of the intermixed samples as the function of exposure time is shown in Fig. 1(b). Compared to the control samples, it is found that the FWHM of samples exposed to an energy density less than 3.5 mJ·mm^{-2} and an exposure time less than 5 min only gives an insignificant change. Spectrum broadening of only 3 meV has been obtained from a sample irradiated with 2.8 mJ mm^{-2} for 1 min. This implies that the quality of the material remains high after a short exposure time at low irradiation energy. In contrast, the spectrum of the samples irradiated with higher pulse energy density and longer irradiation time broaden substantially compared to the as-grown samples. The broadening of the spectrum for samples with their bandgap tuned to large degrees might be due to the loss of carrier confinement in the QW as the band discontinuity between the well and barriers becomes smaller.

Fig. 2 shows the calculated excitonic peak shift with respect to the diffusion length of the QW that characterizes the degree of intermixing in the QW. The plot is generated from a series of bound states calculation of electron and holes confined in the QW using Ben-Daniel Duke's equation in the effective mass approximation [12]. As shown in Fig. 2, the QW confinement becomes weak for a diffusion length of 55 Å, which might result in a broader PL spectrum as observed in Fig. 1(b). The corresponding PL wavelength shift with respect to the as-grown sample at this diffusion length is $\sim$178 nm, which is in good agreement with the highest observed PL shift (at 3.9 mJ mm^{-2}) i.e., $\sim$170 nm.

A qualitative model has been developed to investigate the effect of the laser intensity and the exposure time on bandgap shift. In this model, the point defect density created during the PPAID process is assumed to be uniform in the vicinity of the QW. This approximation is made based on the fact that there is only one QW with very thin width i.e., 55 Å.

The interdiffusion of the group III and group V species is mediated by vacancies. In a radiation enhanced diffusion process, the diffusion coefficient of certain atomic species can be expressed as [13]

$$D_r = (v + v_o)d^2\Gamma_v \tag{1}$$

where D_r is the diffusion coefficient after radiation, v_o is the equilibrium concentration of vacancies, v is the excess vacancies or point defects created by the laser irradiation that effectively assist the diffusion process, Γ_v is the vacancy jump frequency, and d is the jump distance. Since point defect creation is a random multiphoton interaction with atomic lattice, the probability of defect creation is proportional to the number of possible defects that can be created. Assuming that the lattice can only accommodate a certain maximum number of defects ($v_{\rm sat}$), the rate of point defect creation for every pulse can then be expressed as

$$\frac{dv}{dp} = k_r(v_{\rm sat} - v) \tag{2}$$

where p is the number of pulses treated as a continuum variable as the number of pulses involved is large, k_r is the point defect creation constant that depends on irradiation intensity, and $v_{\rm sat}$ is the saturated point defect value. Solving this differential equation gives

$$v = v_{\rm sat}(1 - e^{-k_r p}). \tag{3}$$

This relationship intuitively shows that most of the defects will be created in the early stage of irradiation. Subsequently, there will be fewer defects created when the defects start to build up. This agrees with the experimental observation that the degree of intermixing is not so much dependent on the number of pulses for long irradiation times [14]. Equation (1) can therefore be expressed as

$$\begin{aligned} D_r &= v_o d^2\Gamma_v + v_{\rm sat} d^2\Gamma_v(1 - e^{-k_r p}) \\ &= D_o + D_x(1 - e^{-k_r p}) \end{aligned} \tag{4}$$

where D_o is the diffusion coefficient at thermal equilibrium and D_x is the diffusion coefficient enhanced by the excess vacancies. Both parameters are associated with the QW material while k_r depends on the irradiation intensity. D_r is also temperature-dependent and can be approximated using the Arrhenius equation. The value of this diffusion coefficient and its relevant parameters can be deduced from the PL measurement and the QW bound states calculation.

Fig. 3 shows the experimental and theoretical plot of the PL wavelength shift with respect to the number of irradiation pulses and exposure times. Using (4), the data points can be fitted very well to yield the following parameters for the QW structure after annealing at 625 ° C for 120 s: $D_o = 3.7 \times 10^{-17}$ cm^2·s^{-1}, $D_x = 2.3\times10^{-15}$ cm^2·s^{-1}, and $k_r = 1.6\times10^{-11}, 2.5\times10^{-11}$, and 8.3×10^{-11} per pulse for I =2.8, 3.5, and 3.9 mJ·mm^{-2}, respectively. The parameter k_r indicates the rate of defect creation per laser pulse. Its value increases as the laser intensity increases. The relationship of k_r with respect to intensity is nonlinear and is approximately proportional to I^n, where $n = 4.8 \pm 2$.

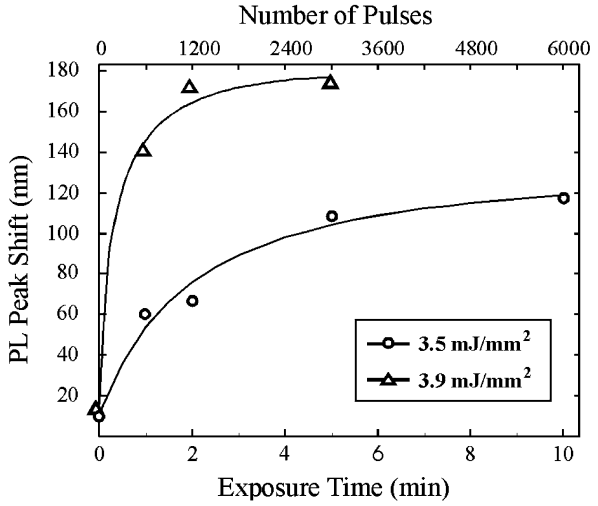

Fig. 3. Experimental (Δ and o) and theoretical (solid line) data for irradiation at 3.5 and 3.9 mJ·mm^{-2}. The shift of the PL wavelength peak is measured with respect to the as-grown sample. The data points at 2.8 mJ·mm^{-2} are omitted for clarity.

III. Spatial Resolution

A sharp bandgap interface transition between the intermixed and unintermixed regions is required for the fabrication of high-density PICs. Time-resolved PL (TRPL) measurements of the intermixed samples have shown that a spatial resolution better than 20 μm, limited by the measurement system, can be obtained [16]. Here, a micro-Raman spectroscopy with a measurement resolution of 2.5 μm was used to investigate the spatial limit resolution of the PPAID process.

The schematic of the sample used in this study is given in Fig. 4(a). In brief, this sample consisted of two sections, i.e., an Au/Si_xN_y masked region and an Si_xN_y section. The sample was irradiated with a pulse energy density of 3.0 mJ·mm^{-2} for 2 min at room temperature and at normal incidence to the surface. The QWI stage was carried out at 625 °C for 120 s using the annealing conditions as mentioned in previous section. After intermixing, the 77K PL spectrum from the masked region shows a wavelength shift of only 2.5 meV compared to that of the as-grown samples, whereas the unmasked region has an additional blue shift of about 60 meV.

To investigate the spatial resolution of the process, micro-Raman spectra were taken in the backscattering configuration in 2.5-μm increments across the interface of the intermixing mask. The sample was positioned and aligned on a high-precision x–y–z translation stage and the measurements were carried out at room temperature. An Ar^+ laser operating at a wavelength of 514.5 nm, 20 mW power, and a spot diameter of $\leq$1 μm was used as excitation source. The penetration depth of the light, calculated from its absorption length in the structure, is about 50 nm below the sample surface.

Due to the laser excitation source and the structure used, the Raman modes with the largest SNR generated in these measurements are those of the InGaAs contact layer, rather than the QW layer. The PPAID process generates point defects not only throughout the active region but also in the cap. The highest concentration of point defects is expected in the cap because of the intensity of the beam and the nonlinear nature of the process. The spatial resolution is determined by the localization with which point defects can be created and the distance they diffuse during the annealing step. Any difference in spatial resolution between intermixing in the cap and QW layers should, to a first approximation, only depend on diffraction of the beam in the region between the cap and the active region, which is a distance of about 1.5 μm. The spatial resolution of intermixing in the InGaAs cap layer is therefore expected to be similar to that in the QW. If the spatial resolution of the process is obtained for the top contact layer, it should be of the same order as that of the QW.

Fig. 5 shows the Raman spectra taken in steps of 2.5 μm across the gold masked boundary. For comparison, the spectrum from an as-grown sample is also included. Since the sample was grown with (100) orientation, only LO phonons are allowed and the transverse optical phonons are forbidden by symmetry selection rules. Three groups of bands can be identified in the spectra. The low frequency range ($<$200 cm^{-1}) band is assigned to the disorder activated longitudinal acoustic (DALA) mode that is found in III-V alloy crystals [17]. The two higher frequency bands in the 210–270- and 300–370-cm^{-1} frequency ranges are identified as optical modes. The 210–270-cm^{-1} band corresponds to the GaInAs-related LO mode. This band is composed of InAs-like (210–235 cm^{-1}) and GaAs-like (240–270 cm^{-1}) LO peaks. The band at around 300–370 cm^{-1} is interpreted as arising from the GaInP LO mode.

Three distinct types of spectra can be observed in Fig. 5.

1) The spectra in Fig. 5(a)–(d) were obtained from the laser-irradiated, and hence, intermixed region. The most distinctive differences between the spectra from this intermixed region compared to those of the as-grown [Fig. 5(j)] and gold-masked region [Fig. 5(f)–(i)] are the shift of GaAs-like LO peak of $\sim$8 cm^{-1} to the lower frequency (line 1) and the reduction of its intensity. The clear shift to a lower frequency and the decrease of intensity of the GaAs-like LO peak are indications for the compositional change in the $In_xGa_{1-x}As$ layer due to the out-diffusion of the Ga and As [18]. The Ga and As vacancies are then replaced by In and P from the $In_xGa_{1-x}As_yP_{1-y}$ layer which is located directly under the $In_xGa_{1-x}As$ layer, thus converting the top $In_xGa_{1-x}As$ layer into $In_xGa_{1-x}As_yP_{1-y}$. This postulate is further supported through the intensity of the GaInP band (300–370 cm^{-1}), which becomes one of the dominant bands in the irradiated region. In these spectra, the DALA modes are also substantially reduced in comparison to those of the as-grown spectrum. This suggests that the disordering evident in the as-grown sample is annealed out during processing.
2) The spectrum of Fig. 5(e) is at the gold masked boundary. Because it is the transitional region, it carries features resembling both the intermixed and as-grown spectra. The GaAs-like mode was found to shift to the lower frequency, similar to the shift in the irradiated region, while the InAs-like LO peak shows a shift of $\sim$4 cm^{-1} to the lower frequency. The GaInP band (300–370 cm^{-1}) starts to increase at this boundary although the intensity

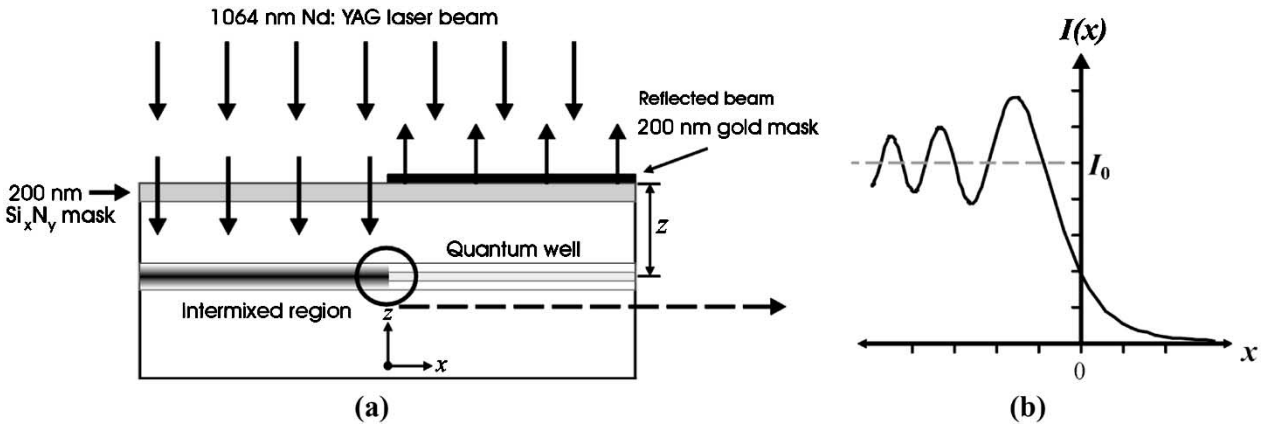

Fig. 4. (a) Schematic of the sample prepared for the spatial resolution experiment. (b) Intensity plot of the diffracted beam in the QW.

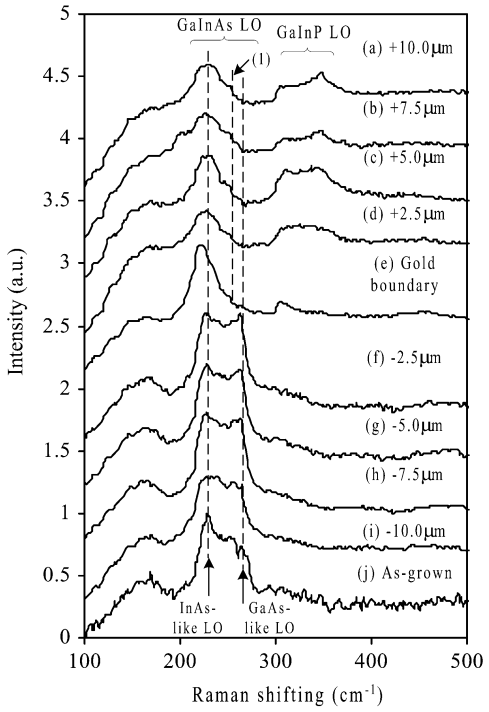

Fig. 5. Raman spectra measured in steps of $+2.5$ μm and -2.5 μm from the gold-masked boundary.

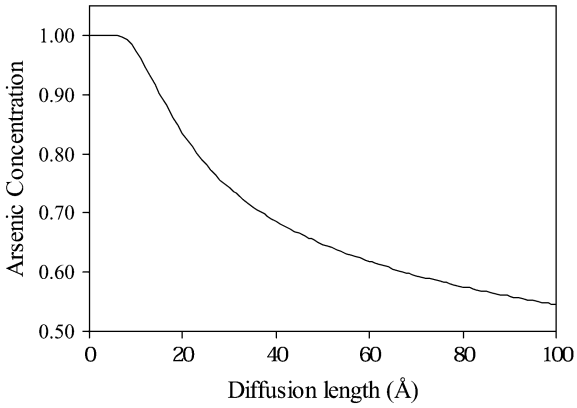

Fig. 6. Arsenic (As) concentration in the middle of the QW.

is lower than that observed in the irradiated region. In addition, the DALA modes could be seen in this spectrum, and they are similar to that of the as-grown sample.

3) The spectra from Fig. 5(f)–(i) were taken from the gold-masked region. In these spectra, the GaInAs LO modes are also the only ones observed. Both the GaAs-like and the InAs-like modes remain distinguished, which agrees well with minimal intermixing observed in this region. Moreover, these Raman spectra, which are very similar to those observed in the as-grown sample, indicate the lack of any noticeable intermixing between the InGaAs cap and the InGaAsP layer after annealing in the masked regions.

This is also clearly evident in the wavelength of the PL peak with a shift of only 2.5 meV compared to that of the as-grown samples. In this region, similar to the as-grown sample, the DALA modes are clearly seen.

After analyzing the Raman spectra, it is clear that the change of the Raman peaks between the intermixed and unintermixed regions takes place between two consecutive Raman spectra measurements, which are 2.5 μm apart. This implies that the resolution of the P-PAID process at the InGaAs cap is better than 2.5 μm. However, as discussed above, the resolution at the QWs should be of the same order of magnitude.

The shift to lower frequency and the decrease of the intensity of the GaAs-like LO mode in the unmasked region are ascribed to the increase in the In concentration (x) due to the interdiffusion of the group III and group V elements between the In_xGa_{1-x} As and $In_xGa_{1-x}As_yP_{1-y}$ layers. Comparing the shifted frequency of the GaAs-like LO mode with the results reported by Sugiura *et al.* and Soni *et al.*, the y composition is approximated to 0.79 [19], [20]. Assuming conservation of the lattice=matching condition $(x = 1 - 0.47y)$ [11], the expected x composition resulting from the intermixing will be $\sim$0.63.

Assuming the lattice-matching condition, the As concentration (y) in the middle of the QW $(z = 0)$ at various diffusion lengths have been calculated (Fig. 6). From the PL measurement at 77 K, the PL shift of the excitonic peak will correspond to a certain value of diffusion length. Then the value of the As composition in the middle of the QW (y) can be obtained. Therefore, using Figs. 2 and 6, the corresponding As concentration (y) due to a PL peak shift of 90 nm obtained from the PL measurement is $\sim$0.83, which is close to that predicted by the Raman spectroscopy measurements.

The spatial resolution of PPAID is difficult to determine experimentally due to the limitation of the measurement system. Therefore, it is interesting to investigate theoretically the limiting resolution of this process and compare it to the existing experimental result. Consider a selective intermixing process whereby part of the sample is masked with a sharp-edge reflecting surface. Due to the diffraction effect, the defect distribution is smeared out laterally. As a result, the point defects concentration will be distributed according to the diffraction intensity pattern as shown in Fig. 4(b). Diffraction effect limits the defect density in vicinity of the mask boundary line. Therefore, a very sharp and discontinuous defect density profile cannot be obtained. This results in a graded diffusion coefficient profile as modeled in (4).

The intensity distribution along the boundary can be calculated by taking into the consideration of the diffraction limit at a sharp edge. A sharp edge here means that there is no reflection along the vertical side of the mask. The 200-nm gold mask is thin enough to serve as a sharp diffraction edge. The distribution of intensity of the pulsed Nd:YAG laser beam can be expressed as [21]

$$I_P(x) = \frac{I_0}{4}\left(\left[\frac{1}{2} - A\left(\sqrt{\frac{2}{\lambda z_t}}x\right)\right]^2 + \left[\frac{1}{2} - B\left(\sqrt{\frac{2}{\lambda z_t}}x\right)\right]^2\right) \quad (5)$$

where z_t is the distance from the mask to the QW active layer assuming a plane wave incidence, x is the horizontal position along the QW active layer [Fig. 4(a)], and λ is the laser wavelength inside the semiconductor material. $A(u)$ and $B(u)$ are Fresnel integrals defined as

$$A(u) = \int_0^u \cos\left(\frac{1}{2}\pi v^2\right)\, dv$$
$$B(u) = \int_0^u \sin\left(\frac{1}{2}\pi v^2\right)\, dv. \quad (6)$$

The wavelength of the laser light λ in the material is given as: $\lambda = \lambda_0/n_R$, where n_R is the effective refractive index of the semiconductor material and λ_0 is the wavelength of the laser in the air. This has the implication that the diffraction pattern will be smaller in favor of higher resolution patterns written into the QW. The plot of intensity distribution is given in Fig. 4(b). This effect together with the phenomenological diffusion coefficient parameters obtained previously are modeled to calculate the two-dimensional (2-D) diffusion profile in the QW. Assuming an isotropic diffusion process, the Fick's second law yields

$$\frac{\partial C(x,z)}{\partial t} = \nabla[D(x,z)\nabla C(x,z)] = \left(\frac{\partial}{\partial x} + \frac{\partial}{\partial z}\right)\left(D(x,z)\left(\frac{\partial C(x,z)}{\partial x} + \frac{\partial C(x,z)}{\partial z}\right)\right) \quad (7)$$

where $C(x,z)$ is the fractional concentration of group III species and $D(x,z)$ is the diffusion coefficient laterally modulated due to different defect density profiles across the region.

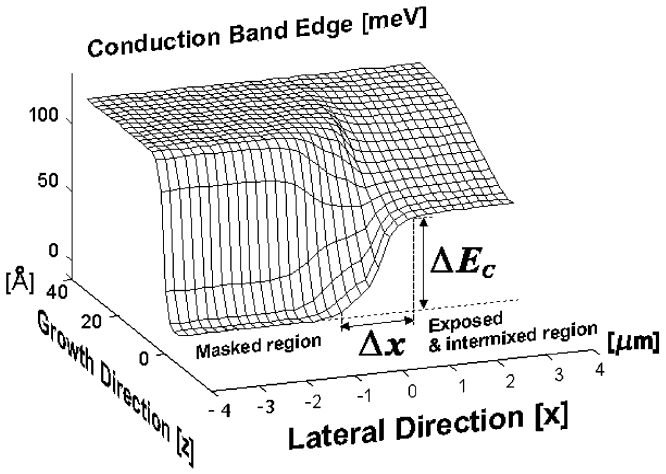

Fig. 7. Half cross section of a selectively masked PPAID process in the QW active layer at a pulse density of 3.9 mJmm^{-2} after 120 s annealing at 625 °C. The mask edge is located at $x = 0$.

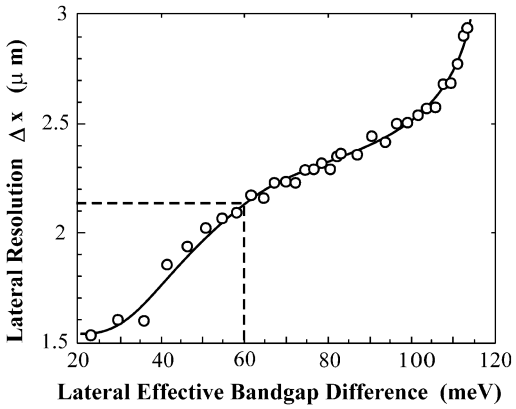

Fig. 8. Calculated lateral resolution (Δx) of PPAID with a 200-nm gold layer as an intermixing mask against the lateral effective bandgap difference. The data points are the result of numerical computation and the curved line is a guide to the eyes only.

The result of finite-element calculation of the QW conduction band edge is shown in Fig. 7. After obtaining the group III lateral concentration profile, the corresponding bound state energy levels can be calculated. The transitional energy between the ground state of the conduction band (CB) to that in the valence band (VB) defines the effective bandgap. With these, the lateral resolution represented by Δx can be calculated. Here, Δx is defined as the distance where the effective bandgap changes from 1% to 99% of the total difference of the effective bandgap between the intermixed and unintermixed regions. The calculated result of the lateral resolution with respect to the lateral bandgap difference is plotted in Fig. 8. It shows that the lateral resolution increases with increasing lateral bandgap difference. The calculated lateral resolution for a 60 meV lateral effective bandgap difference is about 2.15 μm, which is in good agreement to that predicted from the experiment (<2.5 μm).

IV. Material Quality

The effect of laser processing on the material structure was investigated using TEM. Cross-sectional specimens from the as-grown sample together with specimens from the as-irradiated, irradiated, and annealed samples were prepared for TEM

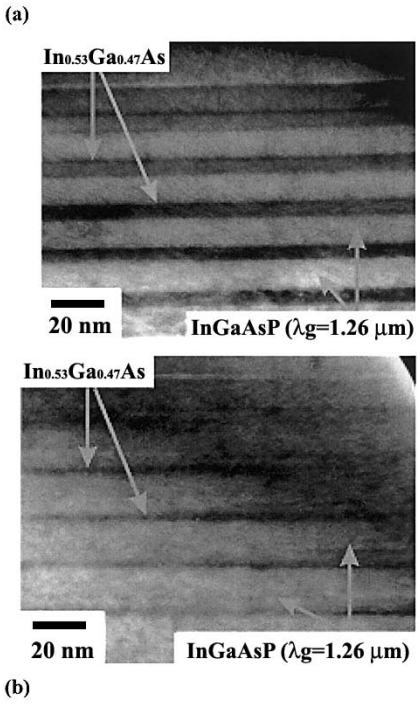

Fig. 9. (a) Bright field image of the as-grown InGaAs–InGaAsP MQW structure. (b) Bright field image of the laser irradiated and annealed sample.

analysis. The laser irradiation was performed with an energy density 3.3 mJ·mm^{-2} for 1200 laser pulses. The samples were annealed using RTP at 625 °C for 120 s. These samples were of similar structure to that described in the previous section, except that the active region now consists of five QWs. TEM measurements were carried out using a JEOL JEM-2010 microscope operating at 200 keV. Cross-sectional specimens were prepared by mechanical polishing, dimple grinding, and, finally, ion milling to electron transparency.

Fig. 9(a) and (b) shows the (001) cross-sectional bright field TEM images of the as-grown, irradiated, and annealed specimens. The InGaAs and InGaAsP layers are well resolved, no damage can be observed, and the well-defined interfaces between InGaAs and InGaAsP are clearly resolved for the as-grown material. The diffraction patterns showed the standard free crystalline patterns of the InGaAs–InGaAsP systems.

There is no discernible difference between the as-irradiated and the as-grown samples. No damage or microstructure can be observed and the diffraction patterns from the as-irradiated specimen are identical to that of the as-grown material, indicating a single-crystal structure. Point defects, especially vacancies and interstitials, are undoubtedly generated during the irradiation, but they were below the resolution limit for detection by the TEM. It is believed that most of the point defects are trapped in the contact and GRIN layers as validated from the investigation of PL spectrum before and after irradiation in Section II. Comparing with the images of the Fig. 9(a) and (b), the contrast at the interfaces is more gradual for the irradiated and annealed specimen than for the as-grown and as-irradiated one, indicating that interdiffusion between the wells and barriers has occurred. The intermixing is confirmed by the blue shifting of the bandgap energy by about 40 meV, as compared to that of the as-grown sample from the PL measurement. The roughness of the interface between the QW and barrier, and the cladding (InP) and the GRIN structure (InGaAsP) might be one of the factors that causes the broadening of the PL spectrum in the intermixed samples as observed in Fig. 1(b).

V. Bandgap Tuned Lasers

To access the quality of the processed material, 50-μm-wide broad-area oxide striped lasers were fabricated from the PPAID intermixed materials together with the as-grown and control samples. In this experiment, the 5-QW laser material, with a structure similar to the multiple QW samples used for TEM analysis, was used. The samples were irradiated with different energy densities for 1200 pulses, and annealed at 590 °C for 120 s. Three sets of oxide stripe lasers with bandgaps tuned by 38, 50, and 82 nm, corresponding to the exposure energy densities of 2.4, 2.7, and 3.4 mJ·mm^{-2}, respectively, have been fabricated. For comparison, lasers have also been fabricated from the as-grown and the control samples. Due to the Gaussian beam profile nature of the Nd:YAG laser, the point defects were not uniformly created over the entire irradiated area of the samples. This resulted in less intermixing around the edges of the samples compared with a more uniform central region. As a result, there was a range of lasing wavelengths obtained from each sample, typically a spread of about 6 nm. In this case, only lasers from the centers of the samples were assessed. The uniformity of the disordering can be improved by using a laser source with a flat-top beam profile.

The spectrum and light–current $(L$–$I)$ measurements were carried out under pulsed current conditions at room temperature. The current pulse width was 3.5 μs and the repetition frequency was 100 kHz (35% of duty cycle). The as-grown and control samples emit at 1551 and 1550 nm respectively, while devices fabricated from the intermixed samples processed by exposing to energy densities of 2.4, 2.7, and 3.4 mJ·mm^{-2} emit at 1512, 1500, and 1468 nm, respectively. The laser emissions are multimode since they are 50 μm wide and gain guided with weak optical confinement and are Fabry–Perot devices.

A summary of laser characteristics from the intermixed and nonintermixed lasers is tabulated in Table I. Since a blueshift in the bandgap energy is achieved here, the free carrier absorption, which is directly proportional to λ [22], [23], is expected to reduce and lead to a decrease in the internal loss $(\alpha_{\rm int})$. In our case, however, an increase in $\alpha_{\rm int}$ is observed. Thus, the increase in threshold current density $(J_{\rm th})$ would only be possible if it is due to the increase in the point defect density, a consequent increase in the concentration of nonradiative recombination centers and the possible formation of extended defects. This effect would also lead to a reduction in the internal quantum efficiency $(\eta_{\rm int})$ as observed.

Our results showed that PPAID can be used to produce very large blueshift in the InP-based QW. However, the use of high-energy laser irradiation often leads to severely damaged material. Above a certain energy, the accumulation of damage clusters causes the annihilation of the PL. These shortcomings could be minimized if we offer optimal control of the laser intensity and the number of laser pulse during the process.

TABLE I
SUMMARY OF THE LASING WAVELENGTH λ, THRESHOLD CURRENT DENSITY $(J_{\rm th})$, INTERNAL QUANTUM EFFICIENCY $(\eta_{\rm int})$, AND INTERNAL PROPAGATION LOSS $(\alpha_{\rm int})$ FOR SAMPLES (a)–(e)

Sample	λ (nm)	$J_{\rm th}$ (kA cm^{-2})	$\alpha_{\rm int}$ (cm^{-1})	η_{int} (%)
A	1551	1.08	38.6	68.0
B	1550	1.10	40.8	66.0
c	1512	1.36	47.4	63.7
d	1500	1.56	48.0	62.8
e	1468	1.88	50.5	59.9

TABLE II
SUMMARY OF LOSS CALCULATED FROM THRESHOLD CURRENT AND SLOPE EFFICIENCIES FROM THE EXTENDED CAVITY LASERS

Extended cavity length (μm)	Best threshold current (mA)	Slope efficiency per-facet (WA^{-1})	Loss (cm^{-1})
0	340	0.152	-
200	360	0.115	3.8
400	384	0.123	4.1
600	438	0.103	5.7

VI. INTEGRATED DEVICES

The ability for using PPAID in the fabrication of a two-section device is demonstrated via the fabrication of oxide-stripe extended cavity lasers. This device consists of two sections, i.e., an active laser region without the bandgap shift and a passive low-loss waveguide region with the bandgap tuned to a higher energy. The InGaAs–InGaAsP MQW laser structure used is similar to that of the structure used in the fabrication of the bandgap-tuned laser. However, the actual QW thickness is slightly larger than the desired value, and, hence the PL peak wavelength of the as-grown material ($\sim$1496 nm at 77 K) is higher than the previous samples. The passive region was exposed to laser energy of 3.6 mJ·mm^{-2} for 1 min and was annealed at 620 °C for 150 s. In this set of devices, the differential bandgap shift between the active and the passive regions is $\sim$162 nm or $\sim$100 meV. The bandgap shift is larger than previously measured. This might be due to a higher annealing temperature and longer annealing time being used to further enhance the interdiffusion rate and minimize the possibility of remaining point defects. The finished lasers have 50-μm oxide stripe windows and were cleaved into lasers with 450 μm of active length and various lengths for the passive section for characterization.

The lasers were tested under similar conditions to the bandgap tuned lasers. The lasing characteristics from the extended cavity lasers for various passive cavity lengths, taken from devices with the best threshold, were recorded in Table II. It is possible to define a relationship in the QW lasers between the all-active laser threshold current $(I_{\rm AALth})$, extended cavity laser threshold current $(I_{\rm ECLth})$, and propagation loss in the passive section (α_p). For an extended cavity laser, with active and passive section lengths of L_a and L_p, respectively, a new threshold current density $J_{\rm ECLth}$ is required. The ratio of the current densities is thus [24]

$$\ln\left(\frac{I_{\rm ECLth}}{I_{\rm AALth}}\right) = \ln\left(\frac{J_{\rm ECLth}}{J_{\rm AALth}}\right) = \frac{\alpha_p}{n\Gamma g_o}\left(\frac{L_p}{L_a}\right) + \frac{1}{n\Gamma g_o L_a}\ln\left(\frac{1}{\kappa}\right) \quad (8)$$

where $J_{\rm AALth}$ is the threshold current density for a laser with a zero-length passive, and κ is the coupling coefficient between the active and passive sections of the laser. The value of $n\Gamma g_o$ was taken to be 30 cm^{-1} [6]. Assuming zero reflection at the active and passive boundary, (8) can be summarized as

$$\ln\left(\frac{I_{\rm ECLth}}{I_{\rm AALth}}\right) = \frac{\alpha_p}{n\Gamma g_o}\left(\frac{L_p}{L_a}\right). \quad (9)$$

The threshold current, the slope efficiency per facet, and the loss in the passive section are tabulated in Table II. The threshold currents of the extended cavity lasers with passive waveguide lengths of 200, 400, and 600 μm increase by about 5.9%, 12.9%, and 28.8%, respectively. The increase of threshold current density for longer cavities might be due to the divergence of the lasing mode within the extended cavity. This reduces the amount of light returning to the pumped laser region. The increase in the threshold current for the extended cavity laser (i.e., 450 μm active/400 μm passive) is extremely favorable when compared to the increase of 45% to 493 mA for the 850-μm all-active laser. As the cavity length of the extended cavity laser increases through increases in the passive waveguide length, the absorption loss makes an increasingly larger contribution to the total loss. The slope efficiency undergoes a corresponding decrease as observed.

The lowest loss was measured in the laser with a 200-μm-long passive region. This loss is comparable to the loss measured

TABLE III
SUMMARY OF THRESHOLD CURRENT DENSITY AND LASING WAVELENGTH TAKEN FROM LASERS WITH A CAVITY LENGTH OF 500 μm OPERATED AT 1.3 TIMES ABOVE THRESHOLD

Energy Density ($mJmm^{-2}$)	Lasing Wavelength (nm)	Wavelength Shift (nm)	Threshold Current Density ($kA\ cm^{-2}$)
0	1539	-	1.24
2.42	1509	30	1.40
2.62	1502	37	1.51
2.81 & 2.98	1490	49	1.58
3.17	1480	59	1.70

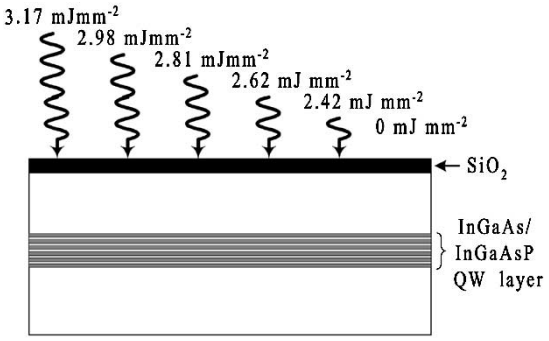

Fig. 10. Schematic diagram showing the amount of energy density used in each section across the single wafer during the laser irradiation.

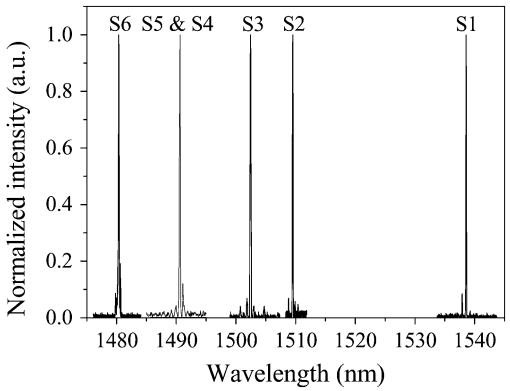

Fig. 11. Lasing spectra of bandgap shifted 50 μm × 500 μm broad-area lasers fabricated from a single sample, which has been intermixed with different pulse energies. The lasing spectrum (S1) from the control area is also included for comparison.

for similar devices processed using a combination of PAID and PPAID process (3.8 cm^{-1} or 16.5 dB cm^{-1}) [6], and IFVD process (4.1 cm^{-1} or 17.8 $dBcm^{-1}$) [25]. It is relatively low if compared to the loss of 28.7 cm^{-1} in the PAID process [23].

A multiple-wavelength laser chip has been fabricated as a means to demonstrate the process capability for the fabrication of multiple-channel and multiple-bandgap PICs. In this experiment, a sample of 8 × 6 mm^2, capped with a 200-nm SiO_2 layer, was exposed to a Q-switched Nd:YAG laser with pulse energy densities varied from 2.42 to 3.17 mJ mm^{-2} for 2 min, as illustrated in Fig. 10. One area of the sample was left unirradiated to act as the control region. After irradiation, the sample was intermixed by annealing at 590 °C for 120 s.

After intermixing, the sample was fabricated into oxide strip lasers with 50-μm contact windows opened on irradiated regions. The lasers were cleaved into devices with a cavity length of 500 μm for characterization. The lasers were tested under pulsed current mode at room temperature. Fig. 11 shows the normalized lasing spectra from the five regions, fabricated from the same sample, which have undergone different degrees of intermixing. The lasing spectra were taken at a current of about 1.3 times above the threshold current. The labels S1–S6 represent pulse energy densities of 0–3.17 mJ·mm^{-2}, respectively.

A total of four different emission wavelengths were observed from the five areas intermixed with different pulse energy densities, where wavelengths of 1509, 1502, and 1480 nm correspond to pulse energy densities of 2.42, 2.62, and 3.17 mJ·mm^{-2}, respectively, and ∼1490 nm to both 2.81 and 2.98 mJ·mm^{-2}. The degree of emission wavelength shift was found to depend on the pulse energy density. Lasers fabricated from the unirradiated region (0 mJ·mm^{-2}) show a lasing wavelength of ∼1539 nm. Therefore, the different wavelengths obtained were due to the intermixing process.

The threshold current density was also determined and is tabulated in Table III. There is a slight increase in the threshold current density for laser S2 compared to that of the control laser (12.9%). On the other hand, for lasers fabricated from regions S3 to S5, the increase of the threshold current density is less than 30%. However, the threshold current density of the lasers intermixed with 3.17 mJ·mm^{-2} increase about 37% compared to the control laser as have observed from the oxide-stripe bandgap tuned laser discussed in Section V.

VII. CONCLUSION

QWI using the PPAID technique has been successfully developed in the InGaAs–InGaAsP material system using a Q-switched Nd:YAG laser with a pulse length of ∼8 ns and a repetition rate of 10 Hz. A differential wavelength shift of over 160 nm has been achieved from InGaAs–InGaAsP heterostructures exposed to 3.9 mJ·mm^{-2} for 5 min. The relationship of the bandgap energy shift with the total pulse energy density and irradiation time has been investigated. Micro-Raman spectroscopy has been used to investigate the spatial resolution of the PPAID process. The measurement showed that a spatial resolution of better than 2.5 μm can be obtained from this process. A theoretical model has been developed to estimate the spatial resolution limit, which comes in a good agreement with the experimental result.

Bandgap-tuned lasers using the InGaAs–InGaAsP laser structure have been successfully fabricated from samples with bandgaps tuned by 38, 50, and 82 nm with exposure to energy densities of 2.4, 2.7, and 3.4 mJ·mm^{-2}, respectively. Results from the laser reveal that the material is still high in quality after the PPAID process. Oxide-stripe extended cavity lasers have been fabricated. Losses as low as 3.8 cm^{-1} or 16.5 dB·cm^{-1} have been measured from the passive waveguide of the extended cavity lasers. A novel direct writing technique to produce different degrees of intermixing in a single wafer has been developed. A total of four laser elements with lasing wavelengths ranging from 1480 to 1512 nm have been obtained from the PPAID intermixed device on a single chip.

REFERENCES

[1] J. H. Marsh, "Quantum well intermixing," *Semicond. Sci. Technol.*, vol. 8, pp. 1136–1155, 1993.

[2] B. S. Ooi, S. G. Ayling, A. C. Bryce, and J. H. Marsh, "Fabrication of multiple wavelength lasers in GaAs/AlGaAs structures using a one-step spatially controlled quantum well intermixing technique," *IEEE Photon. Technol. Lett.*, vol. 7, pp. 944–946, Sept. 1995.

[3] B. S. Ooi, K. McIlvaney, M. W. Street, A. Saher Helmy, S. G. Ayling, A. C. Bryce, J. H. Marsh, and J. S. Roberts, "Selective quantum well intermixing in GaAs/AlGaAs using impurity free vacancy induced disordering," *IEEE J. Quantum Electron*, vol. 33, pp. 1784–1793, Oct. 1997.

[4] H. S. Lim, V. Aimez, B. S. Ooi, J. Beauvais, and J. Beerens, "A novel fabrication technique for multiple-wavelength photonic-integrated devices in InGaAs-InGaAsP laser heterostructures," *IEEE Photon. Technol. Lett.*, vol. 14, pp. 594–596, May 2002.

[5] C. J. McLean, A. McKee, G. Lullo, A. C. Bryce, R. M. De La Rue, and J. H. Marsh, "Quantum well intermixing with high spatial selectivity using a pulsed laser technique," *Electron. Lett.*, vol. 31, pp. 1285–1286, 1995.

[6] B. C. Qiu, A. C. Bryce, R. M. De La Rue, and J. H. Marsh, "Monolithic integration in InGaAs-InGaAsP multiquantum-well structure using laser processing," *IEEE Photon. Technol. Lett.*, vol. 10, pp. 769–771, June 1998.

[7] T. K. Ong, Y. C. Chan, Y. L. Lam, and B. S. Ooi, "Wavelength tuning in InGaAs/InGaAsP quantum well lasers using pulsed photoabsorption induced disordering," *Appl. Phys. Lett.*, vol. 78, pp. 2637–2639, 2001.

[8] B. S. Ooi, C. J. Hamilton, K. McIlvancy, A. C. Bryce, R. M. De La Rue, J. H. Marsh, and J. S. Roberts, "Quantum-well intermixing in GaAs-AlGaAs structures using pulsed laser irradiation," *IEEE Photon. Technol. Lett.*, vol. 9, pp. 587–589, May 1997.

[9] T. K. Ong, B. S. Ooi, Y. L. Lam, Y. C. Chan, Y. Zhou, A. Saher Helmy, and J. H. Marsh, "High spatial resolution quantum well intermixing process in GaInAs/GaInAsP laser structure using pulsed photoabsorption induced disordering," *J. Appl. Phys.*, vol. 87, pp. 2775–2779, 2000.

[10] B. S. Ooi, E. L. Portnoi, C. J. McLean, A. McKee, A. C. Bryce, R. M. De La Rue, and J. H. Marsh, "Direct writing of gratings in GaInAs/GaInAsP quantum well using pulsed laser irradiation," in *Proc. 8th Int. Conf. Indium Phosphide and Related Material*, vol. 8, 1996, pp. 252–255.

[11] S. Adachi, "Material parameters of $In_{1-x}Ga_xAs_yP_{1-y}$ and related binaries," *J. Appl. Phys.*, vol. 53, pp. 8775–8792, 1982.

[12] E. H. Li, "Optical properties of an InGaAs-InP interdiffused quantum well," *IEEE J. Quantum Electron.*, vol. 34, pp. 982–990, June 1998.

[13] R. J. Borg and G. J. Dienes, *An Introduction to Solid State Diffusion*. Boston, MA: Academic, 1988.

[14] C. J. McLean, J. H. Marsh, R. M. De La Rue, A. C. Bryce, B. Garrett, and R. W. Glew, "Layer selective disordering by photoabsorption-induced thermal diffusion in InGaAs/InP based multiquantum well structures," *Electron. Lett.*, vol. 28, pp. 1117–1119, 1992.

[15] W. Hayes and A. M. Stoneham, *Defects and Defect Processes in Nonmetallic Solids*. New York: Wiley, 1985.

[16] S. J. Fancey, G. S. Buller, J. S. Massa, A. C. Walker, C. J. McLean, A. McKee, A. C. Bryce, J. H. Marsh, and R. M. De La Rue, "Time-resolved photoluminescence microscopy of GaInAs/GaInAsP quantum wells intermixed using a pulsed laser technique," *J. Appl. Phys.*, vol. 79, pp. 9390–9392, 1996.

[17] T. Inoshita, "Long-wavelength lattice dynamics of $In_{1-x}Ga_xAs_yP_{1-y}$ alloys," *J. Appl. Phys.*, vol. 56, pp. 2056–2063, 1984.

[18] S. J. Yu, H. Asahi, S. Emura, S. I. Gonda, and K. Nakashima, "Raman scattering study of thermal interdiffusion in InGaAs/InP superlattice structures," *J. Appl. Phys.*, vol. 70, pp. 204–208, 1991.

[19] T. Sugiura, N. Hase, Y. Iguchi, and N. Sawaki, "Raman scattering study of InGaAsP quaternary alloys grown on InP in the immiscible region," *Jpn. J. Appl. Phys.*, vol. 37, pp. 544–549, 1998.

[20] R. K. Soni and S. C. Abbi, "Raman scattering in $In_{1-x}Ga_xAs_yP_{1-y}$ quaternary alloys," *J. Appl. Phys.*, vol. 59, pp. 2184–2188, 1986.

[21] R. Guenther, *Modern Optics*. New York: Wiley, 1990, p. 441.

[22] D. G. Deppe and N. Holonyak Jr., "Atom diffusion and impurity-induced layer disordering in quantum well III-V semiconductor heterostructures," *J. Appl. Phys.*, vol. 64, pp. R93–R113, 1988.

[23] A. McKee, C. J. McLean, G. Lullo, A. C. Bryce, R. M. De La Rue, J. H. Marsh, and C. C. Button, "Monolithic integration in InGaAs-InGaAsP multiple-quantum-well structures using laser intermixing," *IEEE J. Quantum Electron.*, vol. 33, pp. 45–55, Jan. 1997.

[24] J. Werner, E. Kapon, N. G. Stoffel, E. Colas, S. A. Schwarz, C. L. Schwartz, and N. Andreadakis, "Integrated external cavity GaAs/AlGaAs lasers using selective quantum well disordering," *Appl. Phys. Lett.*, vol. 55, pp. 540–542, 1989.

[25] S. D. McDougall, O. P. Kowalski, C. J. Hamilton, F. Camacho, B. C. Qiu, M. Ke, R. M. De La Rue, A. C. Bryce, and J. H. Marsh, "Monolithic integration via a universal damage enhanced quantum-well intermixing technique," *IEEE J. Select. Topics Quantum Electron.*, vol. 4, pp. 636–646, July/Aug. 1998.

Boon-Siew Ooi (M'95–SM'03) received the B.Eng. (first class honors) and Ph.D. degrees from the University of Glasgow, Glasgow, U.K., in 1992 and 1994, respectively. His Ph.D. research was on the fabrication of GaAs–AlGaAs photonic integrated circuits (PICs) using quantum-well intermixing.

He was subsequently a Postdoctoral Research Assistant at the same university, working on III-V based PICs before joining Nanyang Technological University (NTU), Singapore, as an Assistant Professor in July 1996. At NTU, he and his group studied integration processes for InP-based photonic devices and plasma etching of III-V semiconductors, In May 2000, he joined Phosistor Technologies Inc., Pleasanton, CA, as Vice President of Technology, where he and his team were responsible for the development of process and device technologies for InP-based photonic integrated devices. He joined the Department of Electrical and Computer Engineering, Lehigh University, Bethelehem, PA, as an Associate Professor in the fall of 2003. His research interests are primarily in developing monolithic integration process for semiconductor photonic integrated circuits, particularly using quantum-well intermixing and nanofabrication technology.

Dr. Ooi is a member of the Institute of Physics (U.K.) and is a Chartered Physicist. (U.K.).

Teik-Kooi Ong received the B.Eng. and Ph.D. degrees from Nanyang Technological University, Singapore, in 1998 and 2002, respectively. His Ph.D. research was on the study of intermixing effect in III-V quantum-well structures using laser irradiation-induced disordering technique.

He is currently leading the superluminescent light-emitting diode product line in DenseLight Semiconductor, Singapore. His interests include optoelectronics, laser engineering, broad-band light sources, and monolithic integration of optical devices.

Oki Gunawan received the B.Eng. (first class honors) and M.Eng. degrees from Nanyang Technological University (NTU), Singapore, in 1998 and 2000, respectively, both in electrical and electronics engineering, and he is currently working toward the Ph.D. degree in electrical engineering at Princeton University, Princeton, NJ..

At NTU, he worked on theoretical modeling of quantum-well and quantum-dot intermixing. His current research activity is focused on ballistic transport of low-dimensional semiconductor devices in AlGaAs heterostructure at low temperatures.